Rational drug design in photopharmacology

Kobauri, Piermichele

DOI:
10.33612/diss.213323038

Chapter 6

Toward the calculation of light-induced differences in binding affinity with umbrella sampling simulations

The computational methods regularly used in photopharmacology, such as molecular docking and unconstrained molecular dynamics (MD) simulations, allow qualitative predictions or interpretations of light-induced differences in biological activity. In this chapter, we explore the application of umbrella sampling (US) simulations for a posteriori*, quantitative rationalization of the binding affinities of photoswitchable inhibitors. In addition to the intrinsic challenges of implementing such method, preliminary results indicate that an elaborate optimization of the protocol and more extensive simulations are needed to obtain better correlations with the experimental values.*

Piermichele Kobauri, Sebastian Thallmair, Wiktor Szymanski and Ben L. Feringa

6.1 Introduction

It is universally recognized that drug discovery and development are laborious and time-consuming endeavors that need profound reformation.[1,2] Among other strategies, modern computational methods have emerged as effective tools to reduce costs and improve R&D productivity in the pharmaceutical industry.[3–5] Indisputably, the holy grail of computer-aided drug design is to obtain accurate estimations of binding affinity between a ligand and a target, which would greatly benefit hit identification, hit-to-lead and lead optimization.[6,7]

A wide assortment of methods is available for the computational investigation of ligand-target complexes. Molecular docking algorithms, which are commonly used to predict the binding mode of a ligand with its target,[8] are endowed with great speed and simplicity, but their predictions of binding energies (*i.e.*, docking scores) are inaccurate because they neglect effects rising from entropy, together with solvation and structural changes of the target upon binding.[9–11] On the other hand, molecular dynamics (MD) simulations of ligand-target complexes are utilized not only to introduce target flexibility into docking calculations, but also to study *in silico* the thermodynamic and kinetic aspects of ligand binding.[12]

Numerous MD-based methods have been developed for free energy calculations, usually with a trade-off between simplicity of use, computational resources and accuracy of results.[13] The less complicated end point approximation methods,[14] such as molecular mechanics Poisson-Boltzmann surface area (MM-PBSA), overestimate enthalpic benefit and underestimate entropic penalty, because they do not account for water movement or they do not sample all the relevant conformers, respectively.[13] Conversely, the more elaborate free energy perturbation (FEP) methods offer accurate estimations of binding free energy, but are more complex to implement.[15]

Umbrella sampling (US) represents a good compromise for a reliable calculation of the free energy of binding with a rather intuitive and simple approach.[13] By pulling the ligand out of the binding pocket, the attractive force between ligand and target can be evaluated. US employs a sequence of equilibrium simulations (windows) at increasing distance from the binding site, in which harmonic potentials restrain the ligand at fixed positions of the unbinding pathway (Figure 6.1).[16,17] This protocol allows the calculation of the potential of mean force[18] (PMF) along the reaction coordinate (ξ), typically defined as the ligand-target distance. The results from the simulations in the US windows are combined by applying the weighted histogram analysis method (WHAM)[19] to reconstruct the unbiased free energy profile. The binding free energy is estimated as the difference between the maximum and minimum values of the PMF curve.

Despite widespread applications of unbiased MD simulations within photopharmacology,[20] US simulations have been used rarely and only in the context of glutamate receptors.[21,22] In this chapter, we explore the performance of US for different photopharmacological targets. In addition to molecular docking, quantum mechanics and unconstrained MD that we employed thus far in this thesis, we need methods to provide quantitative, reliable

estimations of the light-induced changes in activity of a photoswitchable ligand. Such predictions would empower rational design and interpretation of the observed differences in binding affinities between the photoisomers of a light-switchable drug.

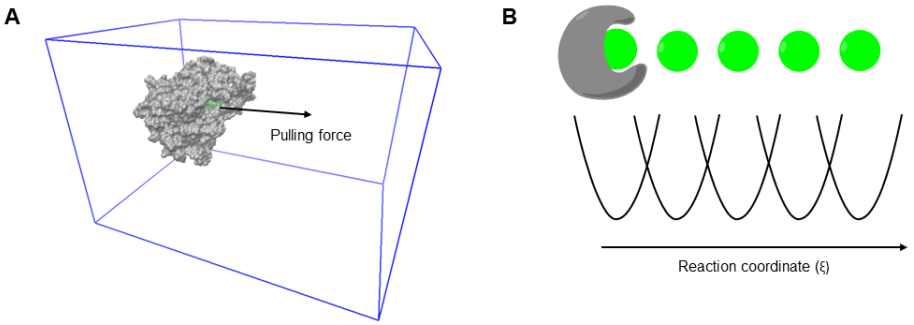

Figure 6.1. Conceptual basis of the US method. (A) The ligand (green) is pulled out of the binding pocket with a harmonic force. (B) US calculations apply harmonic (parabolic) constraints to fix the ligand at certain positions along the reaction coordinate (ξ), *i.e.*, the ligand-target distance.

6.2 Results and discussion

For this study, we chose three azobenzene-containing photoswitchable ligands, targeting histone deacetylase-like amidohydrolase[23] (HDAH, section 6.2.1), histone deacetylase 2[24] (HDAC2, section 6.2.2) and lipoprotein-associated phospholipase A_2[25] (Lp-PLA_2, section 6.2.3). We selected biological targets with solvent-exposed binding pockets, as this feature allows binding of a ligand with no significant conformational changes, thus enabling more reliable estimations of binding affinities through US calculations.[26]

To probe the working range of the method, the starting structures for the US simulations were obtained by computational methods with increasing level of complexity. In all cases, molecular docking was used to generate the binding mode of the ligand. While the docking poses of the HDAH inhibitors could be validated by comparison with the available crystal structure of the complex (PDB ID: 5G3W), the docking poses of the HDAC2 inhibitors were predicted only computationally. Lastly, the initial system configurations for the Lp-PLA2 inhibitors were obtained by a more elaborate protocol, namely induced fit docking (IFD) followed by MD simulations (see Chapter 4). Furthermore, the convergence of the US simulations was assessed by calculating the PMF curves with US windows of 10 and 50 ns.

6.2.1 HDAH

Bordetella/Alcaligenes HDAH,[27] an enzyme homologous to HDACs, catalyzes the deacetylation of acetylated lysine side chains of histone and non-histone proteins, and is a potential target for antibacterial therapies.[23] Compound **1** was reported as a HDAH inhibitor with limited difference in potency between the photoisomers[23] (Figure 6.2).

Although binding to the Zn^{2+} ion could lower the pK_a of the hydroxamic acid,[28] this moiety was kept in its protonated state, in accordance to previous computational studies.[27] Additionally, such simplification allowed to treat the hydroxamic acid uniformly both inside and outside the binding pocket.

Redocking of the co-crystallized ligand enabled the experimental confirmation of the calculated binding mode, with a RMSD of 1.5 Å (Figure 6.5, section 6.6.1). The docking poses of (*E*)- and (*Z*)-**1** were submitted to a 10 ns MD simulation prior to the start of the US protocol. Subsequently, the two isomers were forced to unbind from HDAH by applying a constant pulling force (Figure 6.8). From this trajectory, initial conformations were extracted for US simulations, and the PMF profile was obtained as a function of the ligand-target distance ξ (Figure 6.2).

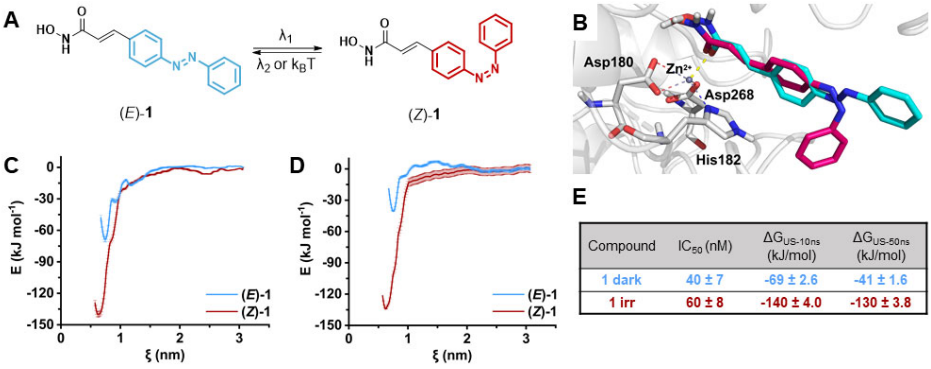

E

Compound	IC_{50} (nM)	$\Delta G_{US\text{-}10ns}$ (kJ/mol)	$\Delta G_{US\text{-}50ns}$ (kJ/mol)
1 dark	40 ± 7	-69 ± 2.6	-41 ± 1.6
1 irr	60 ± 8	-140 ± 4.0	-130 ± 3.8

Figure 6.2. (A) Photoisomerization of compound **1**.[23] (B) Starting structures for the pulling simulations obtained through docking into HDAH (PDB ID: 5G3W). PMF curves obtained for compounds (*E*)- and (*Z*)-**1** with 10 ns (C) and 50 ns (D) US windows. (E) Comparison of experimental IC_{50} values[23] and calculated ΔG values.

In contrast to the experimental IC_{50} values, the US simulations indicated the (*Z*)-isomer of compound **1** as the more active form, with a ΔG_{US} of -130 kJ/mol (Figure 6.2E). Conversely, the (*E*)-isomer was calculated to be a weaker binder of HDAH, with a ΔG_{US} of ca. -40 kJ/mol. These PMF results were in line with the pulling force profile, as the (*Z*)-isomer required a stronger force for its unbinding from the target (Figure 6.8).

The discrepancies between calculations and experiments (Figure 6.2E) are challenging to interpret. Firstly, we exclude that this deviation derives from an inaccurate treatment of dipole moments, which were in good agreement with the experimental values (see section 6.6.2). Since calculations with 10 and 50 ns windows did not show convergence, longer simulation times would be needed to draw informative conclusions. Nevertheless, there might be several reasons for the inaccurate results of our protocol. The treatment of the protonation state of the hydroxamic acid (vide supra) was expected to have a limited impact on the results. Because both isomers contain this moiety, its energetic contributions should be compensated when comparing the binding free energies of the two forms. On the other hand, the crystallization of the **1**-HDAH complex as a dimer could influence the orientation of protein loops, which would require long simulations to equilibrate.

Significantly longer simulations (*e.g.*, tens of μs as enabled by coarse-grained MD simulations[29]) could offer a possible solution to evaluate protein flexibility in a more thoroughly manner.

6.2.2 HDAC2

The HDAC class of enzymes is an established target for chemotherapy,[30,31] and optical control of HDAC inhibition has been reported by our group.[24,25] From these early photopharmacological studies, compound **2** (Figure 6.3) was chosen because of its remarkable difference in activity upon irradiation, as the irradiated, (*Z*)-enriched sample was determined to be > 35-fold more potent than the thermally adapted, (*E*)-containing sample.[24] We envisioned that such large light-induced activation would be easier to appreciate with our computational protocol, as compared to the modest differences between the photoisomers of compound **1**.

Molecular docking was performed into HDAC2 (PDB ID: 4LXZ[32]) to generate the starting configurations for the US simulations. The obtained poses showed a plausible binding mode, with the hydroxamic acid chelating the Zn^{2+} ion (cf. Chapter 4). The docked complexes were then relaxed with a 10 ns MD simulation before starting the pulling and the subsequent US simulations.

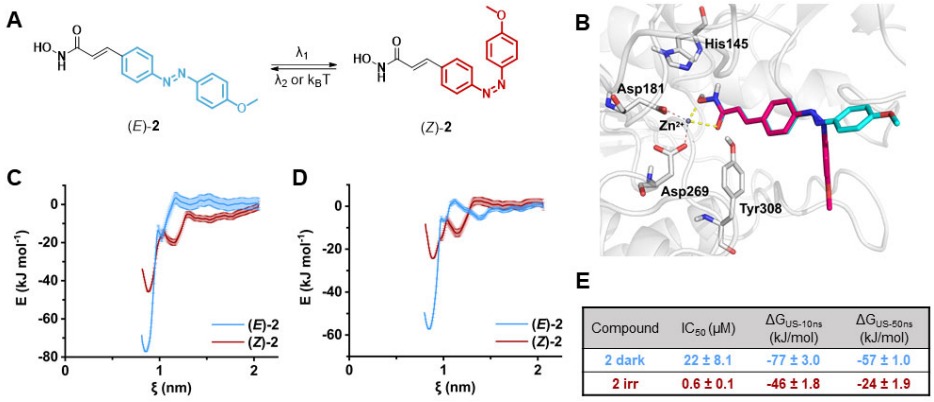

E

Compound	IC_{50} (μM)	$\Delta G_{US\text{-}10ns}$ (kJ/mol)	$\Delta G_{US\text{-}50ns}$ (kJ/mol)
2 dark	22 ± 8.1	-77 ± 3.0	-57 ± 1.0
2 irr	0.6 ± 0.1	-46 ± 1.8	-24 ± 1.9

Figure 6.3. (A) Photoisomerization of compound **2**.[24] (B) Starting structures for the pulling simulations obtained through docking into HDAC2 (PDB ID: 4LXZ). PMF curves obtained for compounds (*E*)- and (*Z*)-**2** with 10 ns (C) and 50 ns (D) US windows. (E) Comparison of experimental IC_{50} values[24] and calculated ΔG values.

The computational results showed similar trends as observed with HDAH (Figure 6.3). A higher free energy of binding was calculated for the (*E*)-isomer of compound **2**, in disagreement with the reported IC_{50} values. The PMF profile displayed the same tendency as the pulling force graph (Figure 6.10). Similarly to the HDAH case, analogous considerations hold true for the HDAC system with regards to the deviation of the calculated binding affinities from the measured inhibition (see section 6.2.1).

6.2.3 Lp-PLA$_2$

The light-controlled inhibition of Lp-PLA$_2$, a potential therapeutic target for atherosclerosis,[33] was recently reported by our group (see Chapter 4[25]). Compound **3**,[25] designed through azologization of the biaryl sulfonamide moiety of compound **4**,[34] acted as a (*Z*)-active inhibitor with a > 10-fold difference in potency (Figure 6.4). The starting structures for the pulling trajectories were adopted from the simulations of Chapter 4, *i.e.*, IFD followed by 100 ns MD simulations.

Studying the complex of compound **3** with Lp-PLA$_2$ allowed us to test whether a better outcome would be obtained when performing US simulations on a system with a buried azobenzene, as opposed to the solvent-exposed azobenzene moieties of the HDAH and HDAC inhibitors. Moreover, in this case we applied the US protocol on the template ligand **4**, thus enabling comparisons with a regular, non-photoswitchable inhibitor.

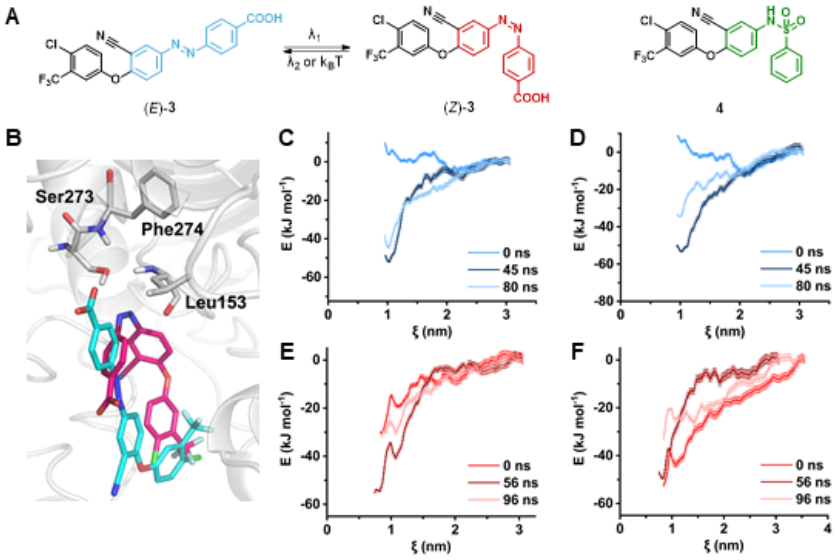

Compound	app. IC_{50}	Snapshot (ns)	$\Delta G_{US\text{-}10ns}$ (kJ/mol)	$\Delta G_{US\text{-}50ns}$ (kJ/mol)
3 dark	> 100 µM	0	3.6 ± 1.2	5.2 ± 1.3
		45	-52 ± 1.6	-53 ± 1.6
		80	-45 ± 1.2	-35 ± 1.3
3 irr	11 ± 9.4 µM	0	-31 ± 1.7	-53 ± 1.5
		56	-55 ± 1.6	-50 ± 2.0
		96	-32 ± 1.4	-33 ± 1.5
4	81 ± 20 nM	/	-62 ± 1.8	-71 ± 0.9

Figure 6.4. (A) Photoisomerization of compound **3**, whose design was based on template ligand **4** (see Chapter 4[25]). (B) Starting structures for the pulling simulations obtained through docking into Lp-PLA$_2$ (PDB ID: 5YEA). PMF curves obtained for compound (*E*)-**3** with 10 ns (C) and 50 ns (D) US windows, for compound (*Z*)-**3** with 10 ns (E) and 50 ns

(F) US windows, and for compound **4** with 10 and 50 ns US windows (G). (H) Comparison of experimental IC_{50} values[25] and calculated ΔG values.

As initial structures for the pulling simulations of the (*E*)- and the (*Z*)-isomer of compound **3**, we chose three snapshots from the 100 ns MD simulations, seeking to sample different binding modes. Snapshots at t = 0, 45 and 80 ns were extracted for (*E*)-**3** (Figure 6.11), while snapshots at t = 0, 56 and 96 ns were extracted for (*Z*)-**3** (Figure 6.13).

Selection of the snapshot highly influenced the US results (Figure 6.4), especially in the case of (*E*)-**3**. When the pulling started from the snapshot at 0 ns, a positive ΔG_{US} was obtained, indicating unfavorable binding. Furthermore, we observed great variability in the estimated binding affinities and in the shape of the PMF profile, depending on the chosen snapshot and on the simulation length of the US windows. Such high influence of the starting structure represents a clear indication of non-convergence of the calculations.[35] On the other hand, ligand **4** was correctly estimated to show the strongest binding to Lp-PLA_2, in accordance with its strong inhibition.[25]

6.3 Conclusion

Going beyond the qualitative predictions of rigid molecular docking and unrestrained MD simulations common in photopharmacology, we attempted to compute quantitative estimations of binding affinities of light-controlled ligands with US simulations. ΔG_{US} values were obtained as the difference between the largest and smallest values of the PMF profile, for photoswitchable ligands targeting HDAH, HDAC2 and Lp-PLA_2. For all three systems, the calculated ΔG_{US} values did not show trends that corresponded to the experimental observations. Future work is needed to optimize and fine-tune the current protocol to achieve improved correlation with a more extensive sample of published biological activity data. One potential strategy would require the implementation of longer MD simulations (100-200 ns at least) to relax the complex before the ligand is pulled out of the target. Alternatively, longer US windows might be necessary to ensure convergence, which is crucial for consistent PMF profiles,[35] and for molecular simulations in general.[36] For this purpose, coarse-grained MD simulations could be used to attain sensibly longer trajectories with reasonable computational cost.

6.4 Acknowledgements

Financial support from the EU Horizon 2020 program (ALERT co-fund No. 713482 for B.L.F.) and the Dutch Scientific Organization (VIDI grant nr. 723.014.001 for W.S.) is kindly acknowledged. P.K. acknowledges the Center for Information Technology of the University of Groningen for their support and for providing access to the Peregrine HPC cluster.

6.5 Author contributions

P.K. and S.T. devised the project. P.K. performed the molecular modeling studies under the direct supervision of S.T. and wrote the manuscript. B.L.F., W.S., and S.T. guided the project and contributed to the manuscript.

6.6 Experimental section

6.6.1 Structure preparation

For general remarks about docking simulations, see Chapter 3. Glide XP[37] was used for HDAH (PDB ID: 5G3W) and HDAC2 (PDB ID: 4LXZ), whereas induced fit docking[38] was used for Lp-PLA2 (PDB ID: 5YEA).

PDB ID: 5G3W[23]

Chain A was selected. The co-crystallized ligand was redocked with root-mean-square deviation (RMSD) = 1.5 Å.

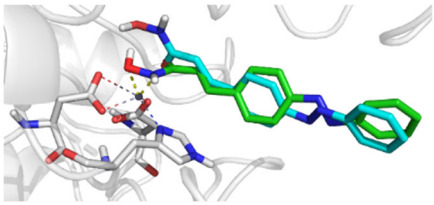

Figure 6.5. Redocking (cyan) of the co-crystallized ligand **1** (green) into HDAH.

PDB ID: 4LXZ[32]

Chain B was selected. Despite its disputed protonation state,[39,40] the hydroxamic acid was considered in its protonated form for simplicity. The Zn^{2+} and Ca^{2+} ions were kept during protein preparation. Also, two specific water molecules (described as WAT1 and WAT2 in a previous study[39]) were kept for 4LXZ. The co-crystallized ligand was redocked with RMSD = 0.6 Å.

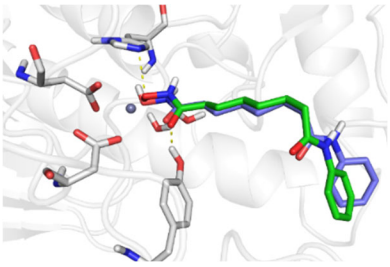

Figure 6.6. Redocking (purple) of the co-crystallized ligand (green) into HDAC2.

PDB ID: 5YEA[34]

Chain B was selected for IFD calculations (see Chapter 4 for more details). During redocking of the co-crystallized ligand, the cNSc dihedral angle was constrained to 80°. This resulted in a successful redocking with RMSD = 1.7 Å. Subsequently, the ligand-protein complexes with (*E*)- and (*Z*)-**3** were submitted to 100 ns of unconstrained MD simulations (see Chapter 4 for more details).

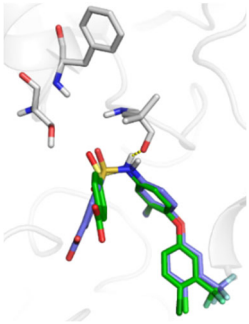

Figure 6.7. Redocking (purple) of the co-crystallized ligand **4** (green) into Lp-PLA_2.

6.6.2 Umbrella sampling

The protocol was obtained by adapting a published procedure.[26]

GROMACS 2018.4 was used for the simulations. The parameter files for the MD simulations were prepared using the tLeap module of Ambertools with the ff14SB force field. Ligand parameters were obtained as Generalized Amber Force Field[41] (GAFF) parameters using the Antechamber module[42] and the AM1-BCC charge method.[43] The dihedral parameters for the azobenzene moiety (see chapter 2) were adapted from a previous study.[44] The calculated dipole moments, *i.e.*, 0 D for (*E*)-azobenzene and 3.5 D for (*Z*)-azobenzene, were in line with the experimental values of 0 D and 3 D, respectively.[45]

The starting structures were immersed in a pre-equilibrated box of TIP3P water molecules, and sodium or chlorine ions were added to maintain electrical neutrality. The simulations parameters were taken from a previous study.[26] The systems were minimized over 50000 steps of the steepest descent algorithm, then they were equilibrated with NVT and NPT simulations at 300 K for 100 ps. During the equilibration steps, the heavy atoms of the Cα atoms of the proteins were kept fixed with a constraint of 1000 kJ/mol. The systems were submitted to additional 10 ns of unrestrained relaxation. Particle mesh Ewald (PME)[46] was used to treat the long-range electrostatic interactions. All bonds were constrained using the LINCS algorithm.

The structures resulting from the equilibration procedure were used as starting points for the pulling simulations. The reaction coordinate (ξ) was defined as the COM distance between the ligands and the specific residues (vide infra). The ligand was dissociated with a pulling simulation, which applied a harmonic force with a spring constant of k = 1500 kJ/mol/nm^2 along the reaction coordinate (ξ). The pulling speed was set as ν = 0.005

nm/ps,[26] for a simulation time of 750 ps. The initial conformations for the US simulations were extracted from the unbinding trajectory with a spacing of 0.05 or 0.025 nm, on the basis of the overlap between adjacent histograms (Figure 6.9). These conformations were subjected to US simulations over 10 and 50 ns, applying a harmonic force with a spring constant of k = 15000 kJ/mol/nm^2 along the reaction coordinate (ξ). The WHAM[19] method was employed to calculate the PMF along the reaction coordinate (ξ), by means of the g_wham command implemented in GROMACS.[47] The error was estimated over 100 rounds of bootstrapping analysis.[48] Pulling force and spacing of the windows along the reaction coordinate were optimized by a trial and error approach for each system.

PDB ID: 5G3W

The starting structures were immersed in a box (9.31 x 9.31 x 13.85 nm^3) of ca. 38000 TIP3P water molecules. The reaction coordinate (ξ) was defined as the COM distance between the ligand and the Zn^{2+} ion of HDAH active site. 54 snapshots were extracted from the unbinding trajectory.

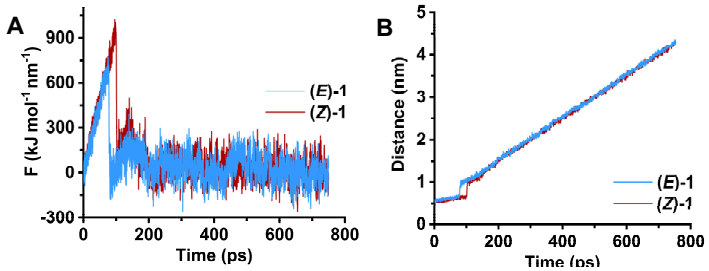

Figure 6.8. (A) Pulling force and (B) displacement of the ligand COM during the pulling simulations of compounds (*E*)- and (*Z*)-**1** away from the binding pocket of HDAH.

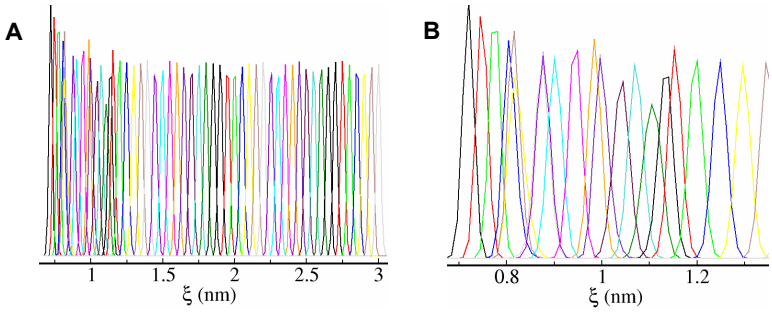

Figure 6.9. (A) Overview and (B) zoomed view of representative histograms of US simulations for compound (*E*)-**1**.

PDB ID: 4LXZ

The starting structures were immersed in a box (9.00 x 9.00 x 13.84 nm^3) of ca. 35000 TIP3P water molecules. The reaction coordinate (ξ) was defined as the COM distance between the ligand and the Zn^{2+} ion of HDAC2 active site. 26 snapshots were extracted from the unbinding trajectory.

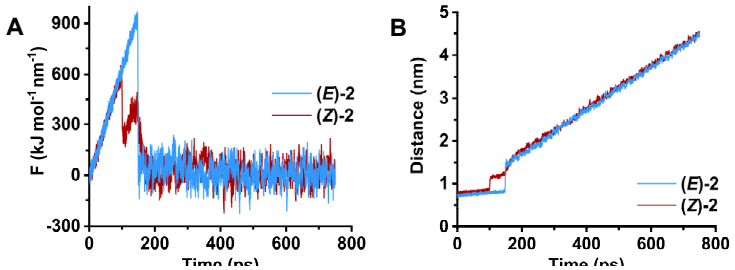

Figure 6.10. (A) Pulling force and (B) displacement of the ligand COM during the pulling simulations of compounds (*E*)- and (*Z*)-**2** away from the binding pocket of HDAC2.

PDB ID: 5YEA

The starting structures were immersed in a box (9.24 x 9.24 x 13.90 nm^3) of ca. 38000 TIP3P water molecules. The reaction coordinate (ξ) was defined as the COM distance between the ligands and Leu159 of Lp-PLA_2 active site. 48 snapshots were extracted from the unbinding trajectory.

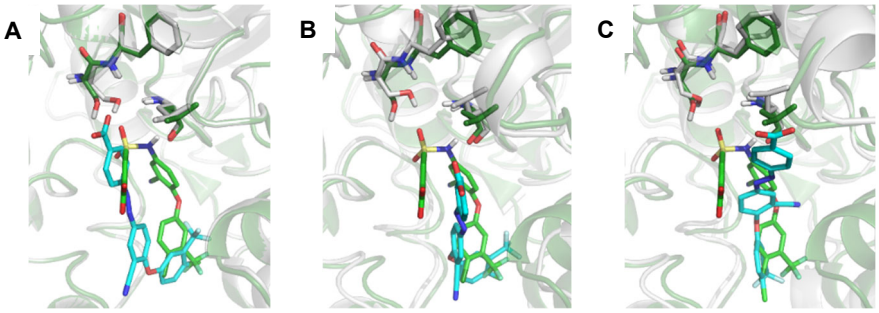

Figure 6.11. Snapshots from the 100 ns MD simulation for compound (*E*)-**3**, which was carried out before the pulling simulation. T = 0 ns (A), 45 ns (B), 80 ns (C). Structural alignment of the snapshot (protein in gray, ligand in cyan) with the initial crystal structure of Lp-PLA_2 (protein in dark green, ligand in green).

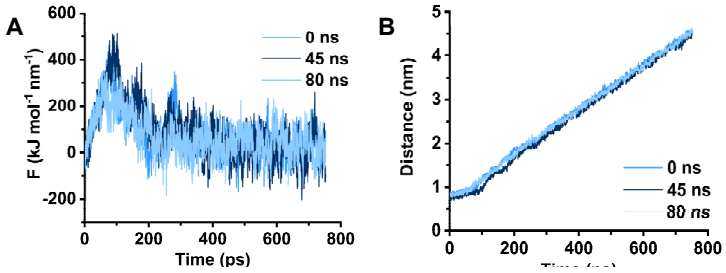

Figure 6.12. (A) Pulling force and (B) displacement of the ligand COM during the pulling simulations of compound (*E*)-**3** away from the binding pocket of Lp-PLA_2.

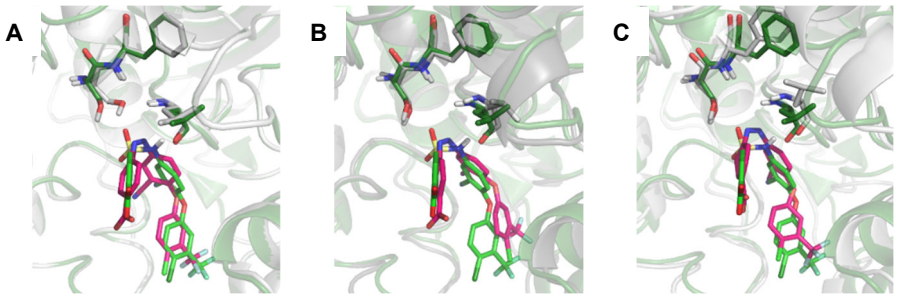

Figure 6.13. Snapshots from the 100 ns MD simulation for compound (*Z*)-**3**, which was carried out before the pulling simulation. T = 0 ns (A), 56 ns (B), 96 ns (C). Structural alignment of the snapshot (protein in gray, ligand in red) with the initial crystal structure of Lp-PLA$_2$ (protein in dark green, ligand in green).

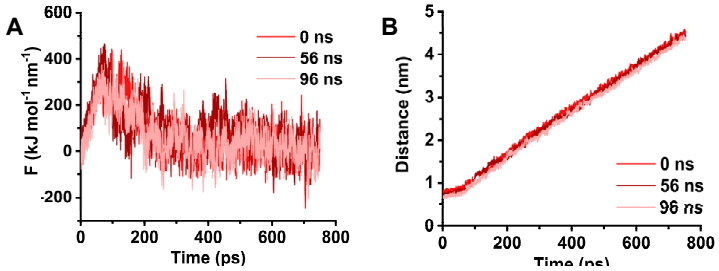

Figure 6.14. (A) Pulling force and (B) displacement of the ligand COM during the pulling simulations of compound (*Z*)-**3** away from the binding pocket of Lp-PLA$_2$.

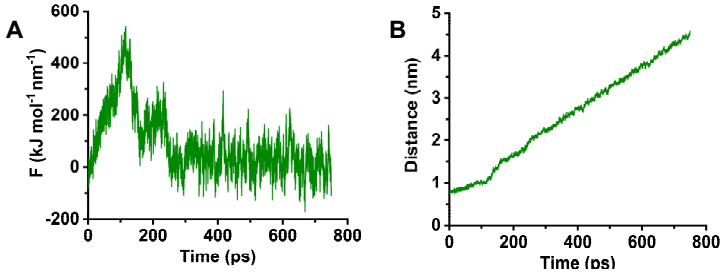

Figure 6.15. (A) Pulling force and (B) displacement of the ligand COM during the pulling simulations of compound **4** away from the binding pocket of Lp-PLA$_2$.

6.7 References

1 S. M. Paul et al., How to Improve RD Productivity: The Pharmaceutical Industry's Grand Challenge, *Nat. Rev. Drug Discov.*, 2010, **9**, 203–214.
2 J. W. Scannell et al., Diagnosing the Decline in Pharmaceutical R&D Efficiency, *Nat. Rev. Drug Discov.*, 2012, **11**, 191–200.
3 S. P. Leelananda and S. Lindert, Computational Methods in Drug Discovery, *Beilstein J. Org. Chem.*, 2016, **12**, 2694–2718.

4 X. Lin et al., A Review on Applications of Computational Methods in Drug Screening and Design, *Molecules*, 2020, **25**, 1–17.
5 J. L. Medina-Franco, Grand Challenges of Computer-Aided Drug Design: The Road Ahead, *Front. Drug Discov.*, 2021, **0**, 2.
6 N. Homeyer et al., Binding Free Energy Calculations for Lead Optimization: Assessment of Their Accuracy in an Industrial Drug Design Context, *J. Chem. Theory Comput.*, 2014, **10**, 3331–3344.
7 Z. Cournia et al., Relative Binding Free Energy Calculations in Drug Discovery: Recent Advances and Practical Considerations, *J. Chem. Inf. Model.*, 2017, **57**, 2911–2937.
8 L. Pinzi and G. Rastelli, Molecular Docking: Shifting Paradigms in Drug Discovery, *Int. J. Mol. Sci.*, 2019, **20**, 4331.
9 D. B. Kitchen et al., Docking and Scoring in Virtual Screening for Drug Discovery: Methods and Applications, *Nat. Rev. Drug Discov.*, 2004, **3**, 935–949.
10 Z. Wang et al., Comprehensive Evaluation of Ten Docking Programs on a Diverse Set of Protein-Ligand Complexes: The Prediction Accuracy of Sampling Power and Scoring Power, *Phys. Chem. Chem. Phys.*, 2016, **18**, 12964–12975.
11 A. Fischer et al., Decision Making in Structure-Based Drug Discovery: Visual Inspection of Docking Results, *J. Med. Chem.*, 2021, **64**, 2489–2500.
12 M. De Vivo et al., Role of Molecular Dynamics and Related Methods in Drug Discovery, *J. Med. Chem.*, 2016, **59**, 4035–4061.
13 B. J. Williams-Noonan et al., Free Energy Methods in Drug Design: Prospects of 'Alchemical Perturbation' in Medicinal Chemistry, *J. Med. Chem.*, 2018, **61**, 638–649.
14 E. Wang et al., End-Point Binding Free Energy Calculation with MM/PBSA and MM/GBSA: Strategies and Applications in Drug Design, *Chem. Rev.*, 2019, **119**, 9478–9508.
15 R. Abel et al., Advancing Drug Discovery through Enhanced Free Energy Calculations, *Acc. Chem. Res.*, 2017, **50**, 1625–1632.
16 J. P. Valleau and T. J.M., Nonphysical Sampling Distributions in Monte Carlo Free-Energy Estimation: Umbrella Sampling, *J. Comput. Phys.*, 1977, **23**, 187–199.
17 J. Kästner, Umbrella Sampling, *Wiley Interdiscip. Rev. Comput. Mol. Sci.*, 2011, **1**, 932–942.
18 R. Benoît, The Calculation of the Potential of Mean Force Using Computer Simulations, *Comput. Phys. Commun.*, 1995, **91**, 275–282.
19 S. Kumar et al., The Weighted Histogram Analysis Method for Free-energy Calculations on Biomolecules. I. The Method, *J. Comput. Chem.*, 1992, **13**, 1011–1021.
20 A. Nin-Hill et al., Photopharmacology of Ion Channels through the Light of the Computational Microscope, *Int. J. Mol. Sci.*, 2021, 22, 12072.
21 R. Numano et al., Nanosculpting Reversed Wavelength Sensitivity into a Photoswitchable IGluR, *Proc. Natl. Acad. Sci. U. S. A.*, 2009, **106**, 6814–6819.
22 Y. Guo et al., Molecular Dynamics Investigation of Gluazo, a Photo-Switchable Ligand for the Glutamate Receptor GluK2, *PLoS One*, 2015, **10**, 1–17.
23 C. E. Weston et al., Toward Photopharmacological Antimicrobial Chemotherapy Using Photoswitchable Amidohydrolase Inhibitors, *ACS Infect. Dis.*, 2017, **3**, 152–161.
24 W. Szymanski et al., Light-Controlled Histone Deacetylase (HDAC) Inhibitors: Towards Photopharmacological Chemotherapy, *Chem. - Eur. J.*, 2015, **21**, 16517–16524.
25 P. Kobauri et al., Biaryl Sulfonamides as Cisoid Azosteres for Photopharmacology, *Chem. Commun.*, 2021, **57**, 4126–4129.
26 S. T. Ngo et al., Effective Estimation of Ligand-Binding Affinity Using Biased Sampling Method, *ACS Omega*, 2019, **4**, 3887–3893.
27 C. Meyners et al., Thermodynamics of Ligand Binding to Histone Deacetylase like Amidohydrolase from Bordetella/Alcaligenes, *J. Mol. Recognit.*, 2014, **27**, 160–172.
28 J. B. Cross et al., The Active Site of a Zinc-Dependent Metalloproteinase Influences the Computed PKa of Ligands Coordinated to the Catalytic Zinc Ion, *J. Am. Chem. Soc.*, 2002, **124**, 11004–11007.
29 N. Singh and W. Li, Recent Advances in Coarse-Grained Models for Biomolecules and Their Applications, *Int. J. Mol. Sci.*, 2019, **20**, 3774.
30 E. Ceccacci and S. Minucci, Inhibition of Histone Deacetylases in Cancer Therapy: Lessons from Leukaemia, *Br. J. Cancer*, 2016, **114**, 605–611.
31 T. Eckschlager et al., Histone Deacetylase Inhibitors as Anticancer Drugs, *Int. J. Mol. Sci.*, 2017, **18**, 1–25.
32 B. E. L. Lauffer et al., Histone Deacetylase (HDAC) Inhibitor Kinetic Rate Constants Correlate with Cellular Histone Acetylation but Not Transcription and Cell Viability, *J. Biol. Chem.*, 2013, **288**, 26926–26943.

33 F. Huang et al., Lipoprotein-Associated Phospholipase A2: The Story Continues, *Med. Res. Rev.*, 2020, **40**, 79–134.
34 Q. Liu et al., Structure-Guided Discovery of Novel, Potent, and Orally Bioavailable Inhibitors of Lipoprotein-Associated Phospholipase A2, *J. Med. Chem.*, 2017, **60**, 10231–10244.
35 W. You et al., Potential Mean Force from Umbrella Sampling Simulations: What Can We Learn and What Is Missed?, *J. Chem. Theory Comput.*, 2019, **15**, 2433–2443.
36 D. L. Mobley, Let's Get Honest about Sampling, *J. Comput. Aided. Mol. Des.*, 2012, **26**, 93–95.
37 R. A. Friesner et al., Extra Precision Glide: Docking and Scoring Incorporating a Model of Hydrophobic Enclosure for Protein−Ligand Complexes, *J. Med. Chem.*, 2006, **49**, 6177–6196.
38 W. Sherman et al., Novel Procedure for Modeling Ligand/Receptor Induced Fit Effects, *J. Med. Chem.*, 2006, **49**, 534–553.
39 J. Zhou et al., Inhibition Mechanism of SAHA in HDAC: A Revisit, *Phys. Chem. Chem. Phys.*, 2015, **17**, 29483–29488.
40 D. Cheshmedzhieva et al., Hydroxamic Acid Derivatives as Histone Deacetylase Inhibitors: A DFT Study of Their Tautomerism and Metal Affinities/Selectivities, *J. Mol. Model.*, 2018, **24**, 2–9.
41 J. Wang et al., Development and Testing of a General Amber Force Field, *J. Comput. Chem.*, 2004, **25**, 1157–1174.
42 J. Wang et al., Automatic Atom Type and Bond Type Perception in Molecular Mechanical Calculations, *J. Mol. Graph. Model.*, 2006, **25**, 247–260.
43 A. Jakalian et al., Fast, Efficient Generation of High-Quality Atomic Charges. AM1-BCC Model: I. Method, *J. Comput. Chem.*, 1999, **21**, 132–146.
44 X. Zheng et al., Molecular Dynamics Simulations of the Supramolecular Assembly between an Azobenzene-Containing Surfactant and α-Cyclodextrin: Role of Photoisomerization, *J. Phys. Chem. B*, 2012, **116**, 823–832.
45 G. S. Hartley and R. J. W. Le Fevre, 119. The Dipole Moments of Cis- and Trans-Azobenzenes and of Some Related Compounds, *J. Chem. Soc.*, 1939, 531–535.
46 U. Essmann et al., A Smooth Particle Mesh Ewald Method, *J. Chem. Phys.*, 1995, **103**, 8577–8593.
47 J. S. Hub et al., G_wham-A Free Weighted Histogram Analysis Implementation Including Robust Error and Autocorrelation Estimates, *J. Chem. Theory Comput.*, 2010, **6**, 3713–3720.
48 B. Efron, Bootstrap Methods: Another Look at the Jackknife, *Ann. Stat.*, 1979, **7**, 1–26.